Fabrication and Characterization of TiO_2 Thin Films and n-TiO_2/p-Si Junction Diodes via Dip Coating Technique

R. Rajeswari [a,*], D. Venugopal [a], P. Jayabal [a] and A. Dhayal Raj[b]

[a] *Department of Physics, Gobi Arts & Science College, Gobichettipalayam, Erode 638452, Tamil Nadu, India*
[b] *Department of Physics, Sacred Heart College, Tirupattur 635 601, Tamil Nadu, India*

Received: 02.06.2020 & Accepted: 29.06.2020

Doi: 10.12693/APhysPolA.138.539 *e-mail: rajimrd@rediffmail.com

The structural and electrical properties of as-prepared and calcinated TiO_2 thin films prepared using the dip coating method are studied. The thin films are deposited by different dip cycles. Subsequently, the samples are used for a p–n junction diode application at room temperature. The films are characterized by XRD, SEM, EDX, UV–Vis spectroscopy, FTIR and I–V to understand the structural and electrical properties. The XRD pattern reveals that the TiO_2 thin films deposited at ambient temperature are amorphous and the films annealed at 450 °C with different dipping cycles are polycrystalline in nature with tetragonal structure. The surface seems to have a uniform sphere-like morphology, with the diameter of ca. 20 nm that is observed from the SEM micrographs. The EDX spectrum confirms the presence of titanium and oxygen in the samples. The electrical behavior of the thin films is studied and it represents that the obtained maximum average conductivity is 10.68×10^{-12} S/cm for the annealed TiO_2 thin films. The diode measurements are taken in darkness and under halogen light. The diode parameters such as ideality factor (n) and barrier height (Φ_b) are calculated using the J-V method

topics: thin films, sol-gel method, I–V characteristics, diode, ideality factor

1. Introduction

The semiconducting transition metal oxides (TMO) are well-known candidates for p–n junction diodes. The physical, chemical, optical, electrical and other properties of the oxide semiconductors can be modified very comfortably as per essentiality by directly tuning a band gap through morphology, doping impurities, ohmic contact formation, etc. [1–3]. Also — due to the longitudinal heterojunction interface, related oxygen vacancies, interstitial defects and strong light trapping [4, 5] on the front panel of the optoelectronic devices — these metal oxides attracted special interest of researchers. Among a variety of semiconducting TMOs, such as TiO_2, ZnO, Fe_2O_3, SnO_2, etc., the TiO_2 semiconductors have become dominant materials in the field of thin film research due to relatively easy construction methods, higher efficiency [6–8] and their semiconducting nature stemming from their extensive band gap energy.

Recently, titanium dioxide (TiO_2) has gained great significance because of its high thermal stability, high dielectric constant, high refractive index, large band gap and low leakage current density. It posseses potential for use in p–n junction diodes, antireflection coating, solar cell catalysis and sensors [9]. In point of fact, TiO_2 has been applied in solar cells [10], diodes [11], gas sensors [12], electrochromic [13] and photochromic batteries [14], pseudo capacitors [15] and in the biomedical field [16]. Formerly, TiO_2 has been synthesized by different techniques such as sputtering, electron beam evaporation, chemical vapor deposition, sol-gel method [17, 18], etc. Among them, the sol-gel dip coating technique has been recruited to grow ultra-thin and high dielectrics on a substrate. This technique has such advantages over other deposition methods as excellent thickness uniformity over large substrate areas, low processing temperature, low impurity content and completely precise thickness control [19, 20].

In our experiment, TiO_2 thin films are prepared using the dip coating method with different dip cycles. Structural and electrical properties of the prepared films are studied using different characterization techniques such as XRD, SEM, FTIR, etc. Further, the p–n junction is formed by taking the TiO_2 as a n-type material on p-type silicon and the fabricated p-Si/n-TiO_2 junction diode characteristics are studied in darkness and under the illumination of a halogen lamp with the use of the J-V method.

2. Experimental procedure

2.1. Materials

Titanium tetra isopropoxide (TTIP, 97%) was purchased from Sigma-Aldrich, dimethylformamide (DMF, 99%), nitric acid (HNO_3, 69%), deionized water, absolute ethanol (C_2H_5OH) and acetylacetone ($CH_3COCH_2COCH_3$) were purchased from Merck. All chemicals are used as received without further purification.

2.2. Preparation of TiO_2 thin films and fabrication of n-TiO_2/p-Si diode

TiO_2 thin films are synthesized by the sol-gel dip coating technique with high precision while maintaining a high optical quality. Titanium (IV) isopropoxide (TTIP) is used as a precursor to prepare TiO_2 sol. A mixture of N–N dimethyl formamide (DMF), ethanol and acetyl acetone is added to titanium (IV) isopropoxide and then diluted by adding a mixture of ethanol and water under continuous magnetic agitation at room temperature. One drop of HNO_3 is added five times for every 10 min to the above-mentioned mixture. The colour of the solution changes from white to transparent TiO_2 sol.

TiO_2 thin films are laid on optically transparent microscopy glass substrates using the dip coating procedure by maintaining the appropriate deposition conditions with a well-defined withdrawal speed. Before dip coating, the glass substrate is washed with deionized water in line with the adequate cleaning procedure. The pre-annealing temperature of the sample with the deposited layer is 150 °C for 30 min, followed by the post-annealing temperature at 450 °C for 1 h. Subsequently, using the dip coating unit, the dipping is carried out for 5, 10 and 15 cycles repeatedly. The deposition conditions maintained to prepare TiO_2 thin films are shown in Table I.

TABLE I

Deposition conditions maintained to prepare TiO_2 thin films

Parameter	Value
substrate	glass
dipping speed	190.00 mm/min
lifting speed	190.00 mm/min
length	25.0 mm
wet time	6 min
dry time	3 min
cycles	5, 10 and 15 cycles
pre-annealing time	30 min
pre-annealing temperature	150 °C
post-annealing time	1 h
post-annealing temperature	450 °C

2.2.1. Silicon wafer cleaning

The n-TiO_2/p-Si diode is prepared using a one-side polished p-type Si wafer. The most essential part in the fabrication of the diode is wafer cleaning because the contaminated surface leads to very poor efficiency. There may be many impurities such as dust, grease, metallic impurities and organic residues on the surface which may result in a number of imperfections on the interface. The carefully performed cleaning steps for silicon wafers are as follows:

- The Si wafer is degreased in boiling acetone and ethanol for 10 min,
- The piranha solution (H_2O_2 + H_2SO_4 in the 2:1 ratio) is prepared for the removal of organic residues,
- The native oxide on the polished surface is removed by applying the HF+H_2O (1:10) solution,
- After each cleaning step, the wafer is thoroughly rinsed in deionized water.

Once the cleaning process is completed, the Si wafer is ready for a coating process. A similar film formation procedure is carried out for the coating of TiO_2 layer on the Si wafer instead of the glass substrate (see Sect. 2.2) and then annealed at 450 °C for 1 h. After the annealing, a better ohmic contact has formed by using the Ag paste. The Ag paste is applied on both surfaces in order to get good solderability, high electrical conductivity, low sheet resistance and good adhesion. Now, the device is dried at room temperature for 5 h for further investigation. Hereafter, the as-deposited samples are named as d, while the annealed samples with 5, 10 and 15 dip cycles are named as d5, d10 and d15, respectively.

3. Results and discussion

3.1. X-ray diffraction pattern

Figure 1 shows the XRD pattern of as-deposited and annealed TiO_2 thin films. The d5, d10 and d15 samples calicinated at 450 °C show the diffraction peaks designating the high crystalline nature of pure TiO_2 thin films. All the diffraction peaks are well-matched with the anatase phase of TiO_2, without any mixed phase like rutile. The positions of the diffraction peaks are in good match with those given by JCPDS Card No. 21-1272 [21] with the lattice constants area: $a = 3.782$Å, $b = 9.513$Å and $c = 2.513$Å. Thus, the formation of pure TiO_2 with tetragonal structure is confirmed. However, the peaks are comparitively broad due to the small size of the crystals. The Debye-Scherrer equation is used to determine the average crystallite size by peak broadening analysis. The anatase film with grain sizes of 7.93 nm, 8.01 nm and 8.18 nm is obtained for d5, d10 and d15 samples for (101) plane, respectively.

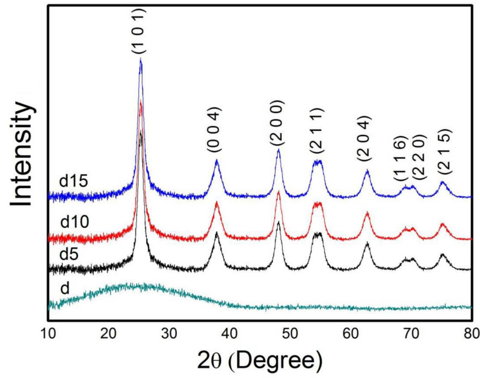

Fig. 1. XRD pattern of as-deposited and annealed TiO_2 thin films.

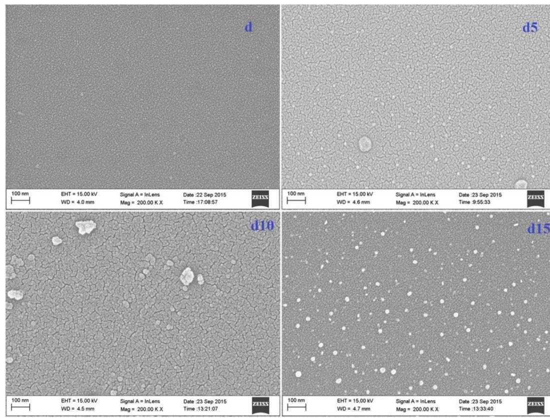

Fig. 2. SEM micrographs of as-deposited and annealed TiO_2 thin films.

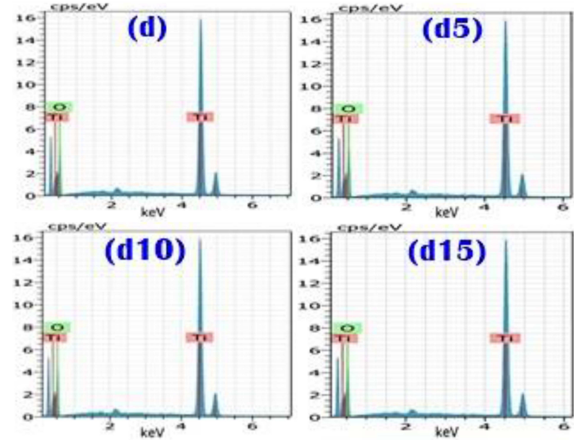

Fig. 3. EDX spectra of as-deposited and annealead TiO_2 thin films.

TABLE II

Wt% and at.% of TiO_2 thin films by EDX.

Sample name	Elements	wt%	at.%	O–Ti ratio
d	Ti	51.34	26.06	2.83
	O	48.66	73.94	
d5	Ti	51.98	26.74	2.73
	O	48.02	73.26	
d10	Ti	52.21	28.43	2.51
	O	47.79	71.57	
d15	Ti	53.08	28.66	2.48
	O	46.92	71.34	

3.2. Morphological analysis

Figure 2 shows SEM images of as-deposited and calcinated TiO_2 thin films. The as-deposited sample d seems to have a smooth surface without any cracks. The d5 and d10 samples show some cracks appearing on the surface of the films. In case of the d15 sample, the surface is very smooth, uniform and crack-free which might be due to the effect of coating cycles. The crack-free d15 sample does not only lack cracks or any other defects in the coatings but its structure and morphology are also more perfect. The surface seems to have a uniform sphere-like morphology, with the diameter of ca. 20 nm [22].

The prepared thin films are subjected to EDX analysis to work out the chemical compositions of the samples. Figure 3 depicts the EDX spectra of as-deposited and annealead thin films. It is very clear that the elemental compostion of all the samples consisting of Ti and O indicates the absence of other elemental impurities. The at% and wt% of the samples are shown in Table II. The O–Ti ratio is calculated as 2.8, 2.7, 2.5 and 2.4 for d, d5, d10 and d15, respectively. From the elemental composition table, it is confirmed that there is an excess of oxygen present in the sample during the preparation. Moreover, the other high intense peak present in the EDX spectra is due to the silicon substrate [23].

3.3. Optical analysis

The UV–Vis absorption spectrum of as-deposited and annealed TiO_2 thin films is shown in Fig. 4. The optical absorption spectra of all the samples in the UV region are due to the wide band gap nature of TiO_2. The absorption edge in the UV region is due to a band to band transition. The optical absorption properties of the semiconductors are related to the energy band gap and the same properties are estimated by the UV–Vis absorption spectra. The optical band-gap E_g of the semiconductor materials is calculated as follows:

$$(\alpha h\nu)^n = A\,(h\nu - E_g)\,,$$

where α, ν, E_g and A are the absorption coefficient, light frequency, band gap energy and absorption constant, respectively, and n depends on the characteristics of the transition in a semiconductor. Here, n is equal to $1/2$ as the material is an indirect-band gap semiconductor.

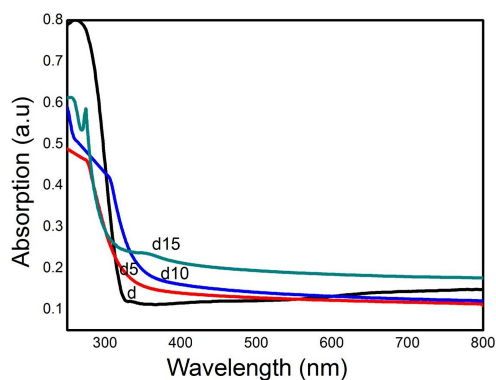

Fig. 4. UV–Vis absorption spectra of as-deposited and annealed TiO_2 thin films.

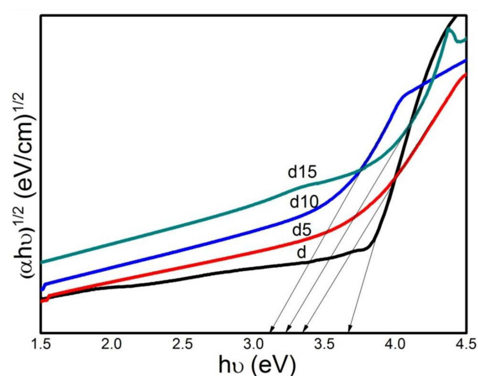

Fig. 5. Band gap of as-deposited and annealed TiO_2 thin films.

In Fig. 5 the intersection point between the extrapolation linear portions gives the value of the energy band gap E_g [24]. The optical band gap of the TiO_2 thin films is estimated as 3.65, 3.41, 3.23 and 3.08 eV for d, d5, d10 and d15, respectively. The estimated band gap value is decreased when the dip cycle is increased. This decrease in the band gap for the d5, d10 and d15 samples is due to the increase in the grain size of the deposited films [25-27].

3.4. Functional group analysis

The vibration behavior of the bonds present in the prepared samples has been investigated through FTIR. Figure 6 shows the FTIR spectra of the as-deposited and annealed TiO_2 thin films. The absorption bands located at 633 cm^{-1} and 566 cm^{-1} for as-deposited and annealed TiO_2 thin films samples are assigned to the Ti–O vibration. This indicates the formation of pure TiO_2 in as-prepared films as well as in the annealed films. The other bands are due to the absence of stretching and bending vibrations of hydroxyl groups and these bands are reduced for the annealed samples [28].

3.5. I–V characteristics

The current-voltage (I–V) measurement is performed by using a 2-point probe connected to a source meter of Keithley Electrometer 6517 B.

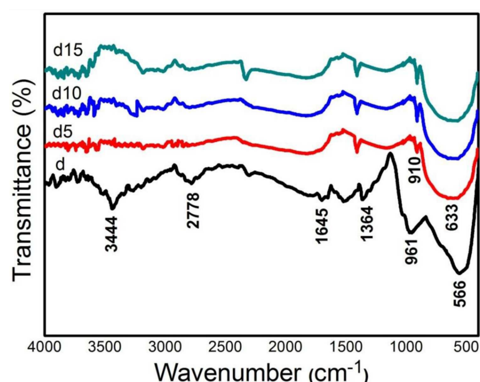

Fig. 6. FTIR spectra of as-deposited and annealed TiO_2 thin films.

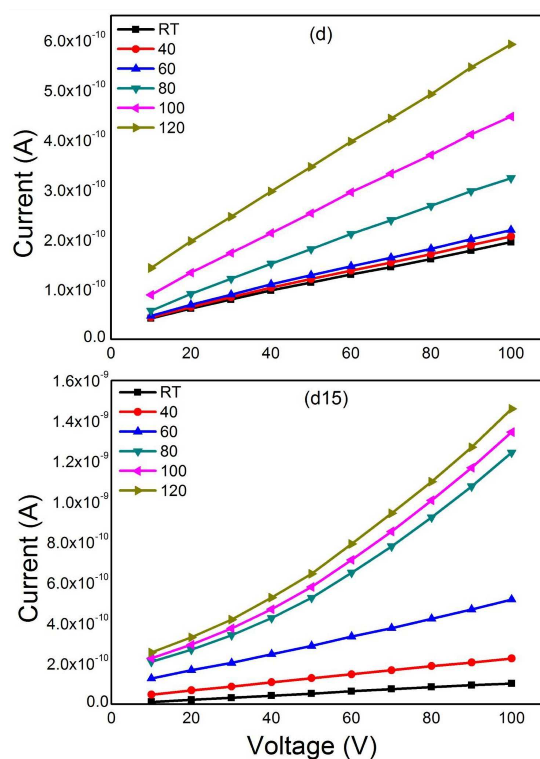

Fig. 7. I–V characteristics of the as-deposited d and annealed d15 TiO_2 thin films.

The I–V characteristics of TiO_2 thin films are tested at six different temperatures: room temperature, 40, 60, 80, 100 and 120 °C. In Fig.7 one can see the current-voltage (I–V) characteristics of the d and d15 TiO_2 thin films. Current values of the synthesized thin films are measured in the voltage range 10–100 V. It can be clearly observed that the current values increase linearly with the applied voltage while all the samples satisfy Ohm's law [29].

The relation between the electric field strength E (V/m) vs current density J (A/cm^2) for the TiO_2 thin films one can see in Fig. 8a, while in Fig. 8b the relation between $\sqrt{E}$ vs $\ln(J)$ is presented. These graphs are plotted only for samples tested at 120 °C for d and d15 TiO_2 thin films.

TABLE III

Electrical parameters obtained from I–V characterization

TiO_2 annealing temperature	Current at 120 °C for 100 V [A]	Conductivity σ [s/m]	Resistivity ρ [Ω m]	Current density J [A/cm^2]
d	5.93×10^{-10}	5.96×10^{-12}	1.67×10^{11}	2.60×10^{-11}
d15	1.46×10^{-09}	10.68×10^{-12}	0.93×10^{11}	4.66×10^{-11}

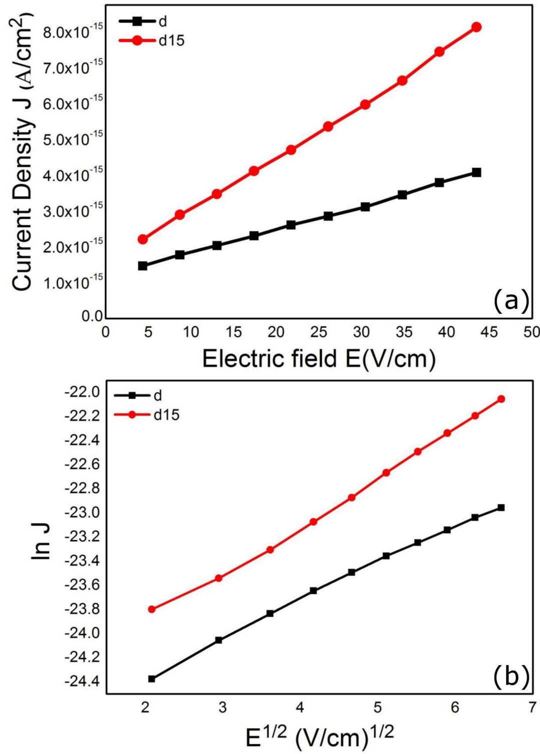

Fig. 8. (a) Electric field vs current density and (b) $E^{1/2}$ vs ln J of TiO_2 thin films.

When the electric field increases, the current density also linearly increases, and for both the films it becomes more linear [30]. The current density and electric field are calculated from the I–V graph.

Furthermore, electrical conductivity σ (S/m) of TiO_2 thin films is found to increase gradually with the increase in annealing temperatures, see Fig. 9. Electrical conductivity of prepared samples is calculated as in [31]. Also, it is found that the increase in annealing temperature decreases the electrical resistivity ρ (Ω m).

Figure 9 shows the average electrical conductivity and resistivity of TiO_2 thin films for different annealing temperatures. The average conductivity of the thin films increases and corresponding resistivity decreases with the increase in annealing temperatures. This increase in electrical conductivity with the increase in temperature indicates the semiconducting behavior of the samples. From the data collected in Table III, the conductivity of the TiO_2 thin film shows improvement from 5.96×10^{-12} S/m (at 0 °C) to 10.68×10^{-12} S/m (at 450 °C).

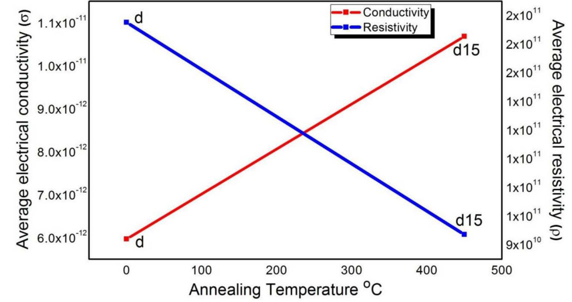

Fig. 9. Electrical conductivity and electrical resistivity of TiO_2 thin films.

On the other hand, the resistivity of thin films decreases as the annealing temperature increases [32]. The as-deposited TiO_2 thin film has the highest resistivity of 1.67×10^{11} Ω m, whereas the annealed TiO_2 thin film has the lowest resistivity of 0.93×10^{11} Ω m. This improvement of conductivity and current density for the annealed sample is due to the increase of grains size and mobility of charge carriers within TiO_2 thin films [33]. Moreover, a very low value of electrical conductivity is due to the excess amount of oxygen present in both samples which is confirmed by the EDX spectra. The oxygen content in the sample determines the value of conductivity in the sample. Samples with oxygen vacancies form titanium suboxides leading to higher conductivity [34]. However, here the process is contrary to the oxygen vacancy which produces no titanium suboxides. Also, in the case of the d sample, there is more excess oxygen so that conductivity is lower as compared to the annealed d15 sample. The increase of the annealing temperature causes a reduced oxygen content and leads to higher conductivity in the d15 sample, as compared to the d sample.

3.6. The diode characterization of n-TiO_2/p-Si

The p–n junction diode is fabricated by the p-type Si with n-type TiO_2 and their functions are calibrated in darkness and under a halogen light source. Figure 10a shows the I–V characteristics of the diode and Fig. 10b shows the semi-logarithmic plot for the current density ln(J) vs voltage V that is represented as the J-V method. The negative top electrode of the devices is represented as the forward bias direction of the current. Measurements from +4 to −4 V bias voltage correspond to the forward to reverse current. The good rectification behavior is observed for the n-TiO_2/p-Si diodes. Note,

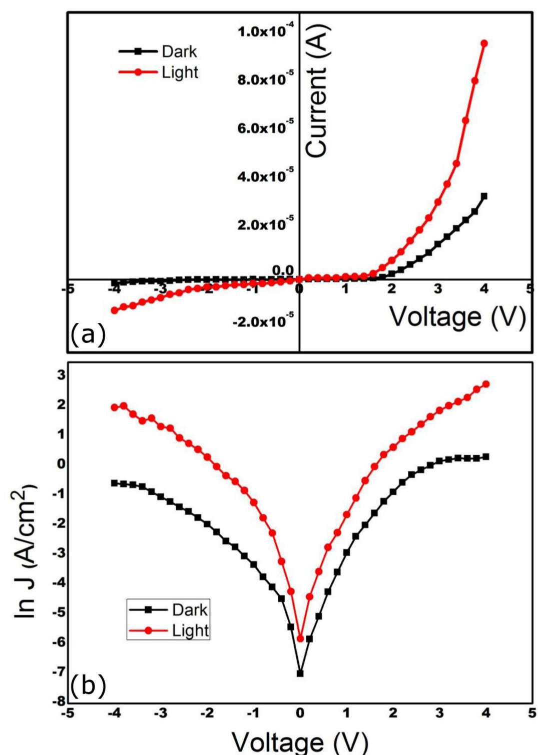

Fig. 10. (a) I–V characteristics and (b) J–V plot of n-TiO_2/p-Si.

however, that the reserve bias current shows a poor saturation current. Here, we also obtained the same result as with the ideal p–n junction diode [35]. From the forward bias condition, we obtained a zero resistivity and in the reverse bias condition infinite resistivity is obtained. The current through the diode can be calculated using the thermionic emission theory as follows [36]:

$$J = J_0 \exp\left(\frac{qV}{nk_{\rm B}T} - 1\right) \tag{1}$$

where J_0 is the reverse saturation current, q is the electron charge, V is the applied voltage, n is the ideality factor, $k_{\rm B}$ is the Boltzmann constant and T is the absolute temperature. The ideality factor n and the reverse bias saturation current J_0 of the diode are determined from the slope. In turn, the intercept of the semi-logarithmic forward bias J–V plot for $V \geq 3k_{\rm B}T/q$ using (1) and the ideality factor n and the barrier height Φ_b can be calculated as follows [37]:

$$n = \frac{q}{k_{\rm B}T}\frac{{\rm d}V}{{\rm d}\ln(J)}. \tag{2}$$

$$\Phi_b = \frac{k_{\rm B}T}{q}\ln\left(\frac{A^*T^2}{J_0}\right) \tag{3}$$

where A^* is the Richardson constant. This value varies by material and doping. The theoretical value for p-type silicon is 32 A/(cm K)^2 [38].

Using the J-V method, the n value for n-TiO_2/p-Si diode is 13.29 in darkness but under the influence of light it decreases to 10.55. This device can be used in solar cells because the increase in luminescence improves the ideality factor. The barrier height Φ_b value for n-TiO_2/p-Si diode is 0.24 eV in darkness but under the light it interestingly increases to 0.38 eV. It is clear that the increase in luminescence improves the barrier height for the system indicating that the diodes can be used in optoelectronic devices. The obtained ideality factor values are more than one (n = 1 for an ideal diode). The non-idealities are due to the presence of a bias-dependent barrier height, the existence of the interfacial thin native SiO_2 layer between the metal (Ag contact) and semiconductor (Si wafer) or generation-recombination currents within the space charge region [39]. Other reasons may be due to the states associated with the defects near the surface of the semiconductor [36, 40], chemical reactions and barrier inhomogeneities [35].

4. Conclusion

The as-deposited and annealed TiO_2 thin films are prepared using the sol-gel dip coating technique. XRD results showed the formation of a pure anatase phase with a tetragonal structure. The SEM analysis reveals that the surfaces of thin films are uniform for 15 dip cycles with a sphere-like morphology. The average diameter of the particle is $\sim$ 20 nm. The EDX spectra indicate the composition with excess oxygen present in the samples. The optical band gap value of the thin films is decreased with the increase of the dip cycle. After annealing, the decrease in the band gap is observed and it can be directly connected to the increase in the structure ordering as observed in the XRD results. The functional analysis reveals that the Ti–O–Ti bands have the tendency to become narrow with the increase of the annealing temperature. This may be due to the breaking of Ti–O–Ti bonds when the annealing temperature increases. The prepared films exposed the semiconducting nature seen in the I–V plot which is favorable for electronic and optoelectronic applications. The ideality factor n and barrier height Φ_b values are n = 13.29, Φ_b = 0.24 eV in darkness and n = 10.55, Φ_b = 0.38 eV under light illumination, respectively obtained for the fabricated n-TiO_2/p-Si diode.

References

[1] S.C. Das, R.J. Green, J. Podder, T.Z. Regier, G.S. Chang, A. Moewes, *J. Phys. Chem. C* **117**, 12745 (2013).

[2] S. Ma, H. Liang, X. Wang, J. Zhou, L. Li, C.Q. Sun, *J. Phys. Chem. C* **115**, 20487 (2011).

[3] L. J. Brillson, Y. Lu, *J. Appl. Phys.* **109**, 121301 (2011).

[4] K.I. Choi, H.R. Kim, K.M. Kim, D. Liu, G. Cao, J.H. Lee, *Sensor Actuat. B Chem.* **146**, 183 (2010).

[5] H.J. Kim, J.H. Lee, *Sensor Actuat. A Phys.* **192**, 607 (2014).

[6] I.S. Cho, J. Choi, K. Zhang, S.J. Kim, M.J. Jeong, L. Cai, T. Park, X. Zheng, J.H. Park, *Nano Lett.* **15**, 5709 (2015).

[7] S.W. Cheong, *Nat. Mater.* **6**, 927 (2007).

[8] X. Lang, A. Hirata, T. Fujita, M. Chen, *Nat. Nanotechnol.* **6**, 232 (2011).

[9] D.S. Jeong, H. Schroeder, R. Waser, *Phys. Rev. B* **79**, 195317 (2009).

[10] B. Li, H. Ren, H. Yuan, A. Karim, X. Gong, *ACS Photonics* **1**, 87 (2014).

[11] C. Osterwald, G. Cheek, J.B. DuBow, V.R.P. Verneker, *Appl. Phys. Lett.* **35**, 775 (1979).

[12] Q. Fu, J. Chen, C. Shi, D. Ma, *ACS Appl. Mater. Interfaces* **5**, 6024 (2013).

[13] J. Meyer, P.R. Kidambi, B.C. Bayer, C. Weijtens, A. Kuhn, A. Centeno, A. Pesquera, A. Zurutuza, J. Robertson, S. Hofmann, *Sci. Rep.* **4**, 5380 (2014).

[14] H.M. Martinez, J. Torres, M.E.R. Garcia, L.D.L. Carreno, *Phys. B Condens. Matter* **407**, 3199 (2012).

[15] A.K. Prasad, D.J. Kubinski, P.I. Gouma, *Sensor Actuat. B Chem.* **93**, 25 (2003).

[16] S.Y. Lin, C.M. Wang, K.S. Kao, Y.C. Chen, C.C. Liu, *J. Sol-Gel Sci. Technol.* **53**, 51 (2010).

[17] A. Zaleska, *Recent Pat. Eng.* **2**, 157 (2008).

[18] D. Byun, Y. Jin, B. Kim, J.K. Lee, D. Park, *J. Hazard. Mater.* **73**, 199 (2000) .

[19] S. Naghibi, A. Jamshidi, O. Torabi, R. Ebrahimi, *Int. J. Appl. Ceram. Technol.* **11**, 901 (2013).

[20] L. Mao, D. Li, H. Dang, Z. Zhang, *Mater. Res. Bull.* **40**, 201 (2005).

[21] F. Bensouici, M. Bououdin, A.A. Dakhel, R.T. Ighil, M. Tounane, A. Iratni, T. Souier, S. Liu, W. Cai, *Appl. Surf. Sci.* **395**, 110 (2017).

[22] G. Balasubramanian, D.D. Dionysiou, M.T. Suidan, V. Subramanian I. Baudin, J.M. Laine, *J. Mater. Sci.* **38**, 823 (2003).

[23] I. Radu, I. Szafraniak, R. Scholz, M. Aleme, U. Gosele, *MRS Proc.* **748**, U11.8 (2002).

[24] F.P. Gokdemir, V.E. Yuzabasioglu, B. Keskin, O. Ozdemir, K. Kutlu, *Adv. Mater. Lett.* **5**, 367 (2014).

[25] S. Gelover, P. Mondragon, A. Jimenez, *J. Photochem. Photobiol. A: Chem.* **165**, 241 (2004).

[26] Z. Wang, U. Helmersson, P.O. Kall, *Thin Solid Films* **405**, 50 (2002).

[27] S. Sen, S. Mahanty, S. Roy, S. Bourgeois, D. Chaumont, *Thin Solid Films* **474**, 245 (2005).

[28] M. Mazur, D. Wojcieszak, J. Domaradzki, D. Kaczmarek, A. Poniedziałek, P. Domanowski, *Mater. Res. Bull.* **72**, 116 (2015).

[29] P.K. Khanna, N. Sirgh, S. Charan, *Mater. Sci. Lett.* **61**, 4725 (2007).

[30] I.H. Tasdemira, O. Vuralb, I. Dokme, *Philos Mag.* **96**, 1684 (2016).

[31] A.H. Chiou1, S.D. Wu, R.C. Hsiao, C.Y. Hsu, *Thin Solid Films* **616**, 116 (2016).

[32] S.B.K. Aydin, D.E. Yildiz, H.K. Çavuş, R. Sahingoz, *Bull. Mater. Sci.* **37**, 1563 (2014).

[33] M. Yilmaz , B.B. Cirak, S. Aydogan, M.L. Grilli, M. Biber, *Super Lattice Microstuct.* **113**, 310 (2018).

[34] A.A. Akl, H. Kamal, K. Abdel-Hady, *Appl. Surf. Sci.* **252**, 8651 (2006).

[35] E.H. Rhoderick, R.H. Williams, *Metal-Semiconductor Contacts*, 2nd Ed., Clarendon Press, 1988.

[36] S.M. Sze, *Physics of Semiconductor Devices*, 2nd Ed., John Wiley and Sons, New York 1981.

[37] K. Akkilic, L. Uzunb, T. Kilicoglu, *Synth. Met.* **157**, 297 (2007).

[38] E. Ugurel, S.Aydogan, K. Serifoglu, A. Turut, *Microelectron. Eng.* **85**, 2299 (2008).

[39] R. Padma, G. Nagaraju, V.R. Reddy, C.J. Choi, *Thin Solid Films* **598**, 236 (2015).

[40] H. Dogan, N. Yildrim, A. Turut, *Microelectron. Eng.* **85**, 655 (2008).